

On the average spin Chern number

Rafael González-Hernández^{1,2,*} and Bernardo Uribe^{3,†}

¹*Departamento de Física y Geociencias, Universidad del Norte,*

Km. 5 Vía Antigua Puerto Colombia, Barranquilla 080020, Colombia

²*Institut für Physik, Johannes Gutenberg Universität Mainz, D-55099 Mainz, Germany*

³*Departamento de Matemáticas y Estadística, Universidad del Norte,*
Km. 5 Vía Antigua Puerto Colombia, Barranquilla 080020, Colombia

(Dated: April 15, 2024)

In this letter we propose the average spin Chern number (ASCN) as an indicator of the topological significance of the spin degree of freedom within insulating materials. Whenever this number is a non-zero even integer, it distinguishes the material as a spin Chern insulator and the number is a topological invariant. If this number is not zero, it indicates that the material has non-trivial spin transport properties, and it lies close to the value of the spin Hall conductivity (SHC) within the bandgap. For materials where spin-orbit coupling (SOC) is small, the ASCN matches the SHC. When the SOC cannot be neglected, both values are non-zero simultaneously. The ASCN is therefore a good complement for the intrinsic contribution of the SHC, and permits to detect topological information of the material which is not possible alone from the value of the SHC.

The investigation of topological phases of matter holds a central position in the landscape of condensed matter physics, tracing its origins to breakthroughs such as the quantum Hall effect and quantum spin Hall effect.¹⁻⁴ The discovery of a constant value within the band gap of the spin Hall conductivity (SHC) in topological insulators presents a compelling challenge, stimulating significant interest and inquiry.⁵⁻⁷ While significant progress has been made in elucidating this issue for 2D topological insulators, where the value becomes quantized in accordance with the definition of the spin Chern number (SCN), this quantization is applicable only in the non-relativistic limit or weak spin-orbit coupling (SOC) interactions.^{8,9} Nevertheless, a critical question remains unresolved, particularly concerning 3D topological insulators.¹⁰ The constant value of the SHC within the band gap eludes a comprehensive explanation, even in the non-relativistic limit.

The conventional approach to topological features of matter typically focus on the exploration of electronic band structures.^{11,12} However, when considering the incorporation of spin quantum degree of freedom, an additional step is required: the projection of spin operator onto the valence electronic states.¹³⁻¹⁵ This process produces the spin spectrum, with the intrinsic topology originating from the nontrivial spin Chern number, independently of the SOC. This spin topology classification approach provides robust topological invariants for studying the spin transport response of quantum systems.^{14,16}

In this letter, we introduce the concept of average spin Chern number (ASCN) as a strategic tool to unravel the nature of SHC within the bandgap in 3D topological insulators. We show that the ASCN may offer valuable insights for the information underlying the SHC in insulator materials, thus indicating the interplay between spin properties and topological features in such systems. By exploring the connection between SHC and ASCN,

our work aims to contribute to a deeper understanding of spin transport phenomena in 3D topological insulators.

In an insulator, the valence states forms a complex vector bundle that is known by the name of *Bloch bundle*. The Bloch bundle is endowed with the action of the group of crystal symmetries and moreover, it may possess time reversal symmetry, or a composition of time reversal symmetry with a rotation, inversion or a translation in the magnetic case.¹⁷ Incorporating SOC implies that the Bloch bundle is endowed with the action of the lift of the crystal symmetries to the spin group, and that time reversal operator squares to -1 .

All these symmetries endow the Bloch bundle with a rich variety of topological invariants, some of them related to magneto-electric properties of the crystal.^{18,19} Among those topological invariants we may mention the Chern-Simons axion coupling term and the Chern classes.^{20,21} The first one is equivalent to the Kane-Mele invariant in the presence of time reversal symmetry,^{22,23} and this invariant gives the indication of a strong topological insulating phase.

When taking into consideration the spin operator S_n in any direction n , we see that the Bloch bundle is moreover endowed with the symmetry induced by this operator once it has been projected to the valence states. In other words, if P is the projection operator into the valence states, the operator PS_nP defines a Hermitian operator on the Bloch bundle.¹³ This projected spin operator PS_nP is a Hermitian operator on the valence states whose eigenvalues lie in between -1 and 1 (in $\hbar/2$ units). In systems with time reversal symmetry we may separate the positive eigenvectors from the negative ones in all but finite points in momentum space.¹³ The points where they cannot be separated are the ones on which the projected spin spectrum includes zero as an eigenvalue. These points are called spin Weyl points (SWP) and their presence or absence have direct topological con-

sequences within the material, particularly evident in the spin transport response.¹⁶

For any choice of oriented coordinate axes $\{a, b, c\}$ we may determine the first Chern numbers

$$c_{1,ab}^{S_n,+}(l) \text{ and } c_{1,ab}^{S_n,-}(l) \quad (1)$$

of the positive and negative eigenvectors of the projected spin operator PS_nP restricted to the reciprocal space planes $k_c = l$ for $l \in [0, 2\pi]$. Since there are only a finite number of SWPs, then these Chern numbers are defined for all the planes $k_c = l$ except for a finite number of them where the SWPs lie.

The spin Chern number is thus:

$$c_{1,ab}^{S_n}(l) := c_{1,ab}^{S_n,+}(l) - c_{1,ab}^{S_n,-}(l), \quad (2)$$

and it is a well defined integer for all but finite number of k -planes. For systems on which the first Chern number is zero on all planes, the spin Chern number is always twice the value of the Chern number of the positive eigenvectors. This is the case on systems with time reversal symmetry.

In order to obtain a number for each spin direction and each plane direction, we propose to consider the *average spin Chern number* (ASCN) across all planes in the reciprocal space:

$$\bar{c}_{1,ab}^{S_n} = \frac{1}{2\pi} \int_0^{2\pi} c_{1,ab}^{S_n}(l) dl. \quad (3)$$

For a set of axes with the opposite orientation $\{b, a, c\}$ we define the ASCN as:

$$\bar{c}_{1,ba}^{S_n} := -\bar{c}_{1,ab}^{S_n}. \quad (4)$$

The ASCN has the following properties (see the Supplemental Material²⁴ for an explanation):

1. When SOC is disregarded, the intrinsic contribution of the spin Hall conductance (SHC) is a multiple of the ASCN:

$$\sigma_{ab}^c = -e\pi \cdot \bar{c}_{1,ab}^{S_c} \quad (5)$$

whenever abc is a base in a cartesian coordinate system.

2. The ASCN is not-linear on the spin direction n .
3. If the ASCN is zero in all spin directions then the material is a spin insulator.
4. If the ASCN is a non-zero even integer, it means that the projected spin operator PS_nP has no SWPs. Therefore the material is a spin Chern insulator in all directions of the spin except in a curve of codimension 1, where there is a change of phase, or when the ASCN is zero.

5. If the ASCN is non-zero in some spin direction, then the spin Chern number is non-zero on some plane. This will imply that the SHC is also not zero.
6. If the Chern-Simon axion coupling term is non-zero, and the positive spin projection eigenvectors are mapped to the negative ones, then the ASCN is non-zero in all spin directions but a codimension 1 curve.
7. In strong topological insulators ($\mathbb{Z}_2 = 1$) the value of the ASCN $\bar{c}_{1,ab}^{S_n}$ determines the spin Chern numbers on the planes $k_c = 0$ and $k_c = \pi$ with abc a base. If $2s < \bar{c}_{1,ab}^{S_c} < 2s + 2$ for $s \in \mathbb{Z}$ then the spin Chern numbers $c_{1,ab}^{S_n}(0)$ and $c_{1,ab}^{S_n}(\pi)$ on the planes $k_c = 0$ and $k_c = \pi$ are $2s$ and $2s + 2$ (not necessarily in this order).

The ASCN is therefore a good indicator for the existence of topological properties of the spin spectrum. It is not in general a topological invariant, in the sense that adiabatic deformations of the Hamiltonian will not leave the ASCN fixed, but a non-zero value of the ASCN indicates the existence of topological invariants of the projected spin operator across some fixed planes in momentum space.

Whenever the ASCN is an even integer, then this number is indeed a topological invariant of the system. This number indicates that the material has a constant spin Chern number across all parallel planes in a fixed spin direction, and these numbers does not change on adiabatic deformations of the Hamiltonian. This particular phase is also recognized as the 3D quantum spin Hall insulator state, in analogy with the 2D.^{25,26}

When the ASCN is non-zero, it implies a corresponding non-zero value for the SHC, and the intensity of the SHC is linked to the magnitude of the ASCN. In Table I we have collected the values of the ASCN and the SHC for different materials with topological properties. It is important to note that their values are related, and moreover, that we can deduce from the value of the ASCN the fact that α -BiBr has projected spin gap and therefore it is a quantum Hall spin insulator. Also we deduce that and that the spin Chern numbers for $\text{MnBi}_6\text{Te}_{10}$ are -6 and -4 in on the planes $k_z = 0$ and $k_z = \pi$.

The ASCN can also be calculated in Weyl semimetals. The occupied states restricted to a plane $k_c = l$ are gapped except where the energy meets the Fermi energy, which happens only at a finite number of points. Moreover, the projected spin operator is always gapped for the planes $k_c = l$ except for a finite number of planes. Hence the SCN is well defined for all planes $k_c = l$, except for a finite number of planes where Weyl points are located. In the case of Weyl semi-metals the value of the ASCN will be very close to the one of the SHC since the eigenvalues of the projected spin operator will be close to 1 and -1 .

Note that the *average Chern number* (ACN) can also be define on the occupied states:

$$\bar{c}_{1,ab} = \frac{1}{2\pi} \int_0^{2\pi} c_{1,ab}(l) dl. \quad (6)$$

Here $c_{1,ab}(l)$ is the first Chern number of the occupied states restricted to the plane $k_c = l$. In this case it follows that the AHC is a multiple to the ACN, no matter what the Fermi energy level is. In formulas we have

$$\sigma_{ab} = \frac{e^2}{h} 2\pi \cdot \bar{c}_{1,ab}, \quad (7)$$

and therefore the AHC is quantized on Chern insulators.

So we can interpret the AHC as the average contribution of the Chern numbers across parallel planes in reciprocal space. When the ACN is an integer, it means that the material has an energy gap and that the Chern number is constant across parallel planes. If the ACN is non-zero, it means that there are planes in momentum space where the Chern numbers is non-zero, and a contribution to the anomalous Hall conductance is present. This topological contribution is linked with the distance in momentum space of the Weyl points in Weyl semimetals.^{27,28}

We have carried extensive calculations for the ASCN and its relation to the SHC in the 3D BHZ model of four bands.²⁹ The BHZ Hamiltonian can be written as (see Supplementd Material²⁴):

$$H(\mathbf{k}) = M\tau_3\sigma_0 + A\tau_1\sigma_3 + C\tau_2\sigma_0 + D\tau_1\sigma_1, \quad (8)$$

with

$$M = M_0 - B_0 (\cos(k_x) + \cos(k_y) + \cos(k_z)), \quad (9)$$

$$A = A_0 \sin(k_x), \quad (10)$$

$$C = C_0 \sin(k_y), \quad (11)$$

$$D = D_0 \sin(k_z), \quad (12)$$

spin matrices $S_x = \tau_0\sigma_1$, $S_y = \tau_3\sigma_2$ and $S_z = \tau_0\sigma_3$ and time reversal $\mathbb{T} = i\tau_0\sigma_2\mathbb{K}$ where \mathbb{K} is complex conjugation.

The energy gap closes whenever $\frac{M_0}{B_0} \in \{-3, -1, 1, 3\}$, and it is a non-trivial insulator only for $-3 < \frac{M_0}{B_0} < 3$.¹⁶

The SOC could be interpreted as the matrix $D\tau_1\sigma_1$ and its intensity as the value of D_0 . In Fig. 1 a) the ASCN $\bar{c}_{1,xy}^{S_z}$ has been plotted with respect to the value of $\frac{M_0}{B_0}$, together with the SHC σ_{xy}^z for different values of D_0 .

It is important to note that the ASCN remains unaffected by the value of D_0 , serving as a direct measure of the SWP's distance. Notably, in the case of $D_0 = 0$, the ASCN aligns with the SHC and the intensity of the SHC decreases for bigger D_0 ; however, both the ASCN and the SHC retain non-zero values simultaneously.

Choosing a generic direction $n = (\alpha, \beta, \gamma)$ of the spin S_n , we see that the SWPs are located at the points in

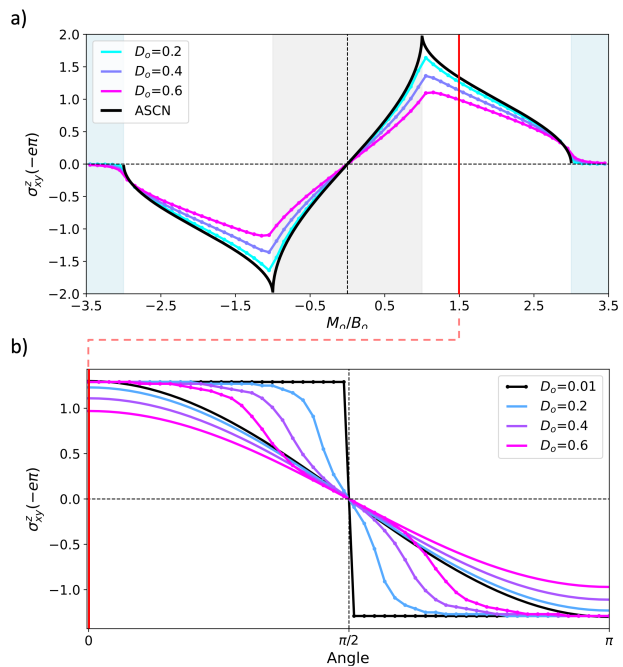


FIG. 1. Comparison of SHC with the ASCN in the 3D BHZ model using various computational and theoretical approaches. a) Results obtained from the Kubo formula Eqn. (12)²⁴ of the SHC σ_{xy}^z for different values of D_0 (in colors), and the ASCN $\bar{c}_{1,xy}^{S_z}$ of (3) in reciprocal space (black line), are plotted against the $\frac{M_0}{B_0}$ parameters. The shaded areas represent different phases: the blue region denotes the trivial phase, while the white and gray areas indicate the strong and fragile phases, respectively. b) Comparison of the SHC $n \cdot (\sigma_{xy}^x, \sigma_{xy}^y, \sigma_{xy}^z)$ (lines without dots) with the ASCN $\bar{c}_{1,xy}^{S_n}$ (lines with dots) for the spin S_n where $n = (\sin(\theta), 0, \cos(\theta))$ and $0 \leq \theta \leq \pi$. Here we go from S_z to S_x and finish in S_{-z} . The graph a) is at angle $\theta = 0$ and the graph b) is at $\frac{M_0}{B_0} = 1.5$. The red vertical line in the graphs represent the same information. The strength of spin-orbit coupling (D_0) is measured in electron volts (eV).

momentum space that solve the following system of equations (see Supplemental Material²⁴):

$$\cos(k_x) + \cos(k_y) + \cos(k_z) = \frac{M_0}{B_0}, \quad (13)$$

$$\gamma A_0 \sin(k_x) + \alpha D_0 \sin(k_z) = 0, \quad (14)$$

$$\gamma C_0 \sin(k_y) - \beta D_0 \sin(k_z) = 0. \quad (15)$$

Whenever $-3 < \frac{M_0}{B_0} < -1$ and $1 < \frac{M_0}{B_0} < 3$ there is only one pair of opposite SWPs, and for $-1 < \frac{M_0}{B_0} < 1$ there are two pairs of opposite SWPs.

In Fig. 1 b) we have plotted the ASCN $\bar{c}_{1,xy}^{S_n}$ and the SHC for values of $n = (\sin(\theta), 0, \cos(\theta))$ where $0 \leq \theta \leq \pi$. The ASCN only depends on the location and chiralities of the SWPs for each choice of n , while the SHC can be calculated by the expression

$$\sigma_{xy}^n = \sin(\theta)\sigma_{xy}^x + \cos(\theta)\sigma_{xy}^z. \quad (16)$$

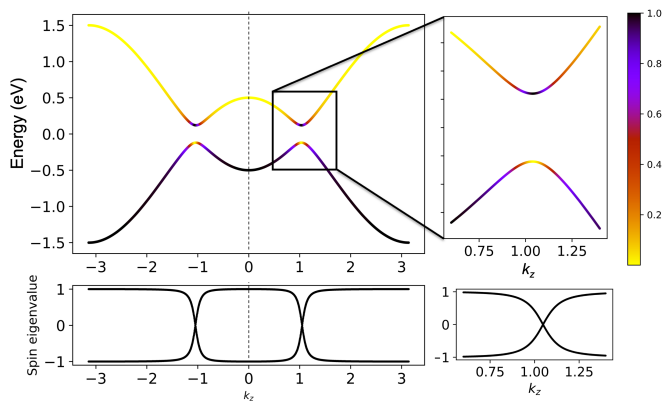


FIG. 2. Graph of the projection of the positive projected spin S_z eigenvector into the valence and conduction bands on the 3D BHZ model at the k_z axis on the point $(k_x, k_y) = (0, \pi)$ for $\frac{M_0}{B_0} = 0.5$, $A_0 = C_0 = 1$, $D_0 = 0.11$. The SWPs are located on this axis and the graph of the projected spin eigenvalues lies at the bottom. The top graphs are the degenerate energies of the four bands, and the color represents the square of the norm of the projection of the positive spin eigenvector of PS_zP into the valence and the conduction states respectively. If ϕ is the positive eigenvector of PS_zP , then the color on the upper bands represent the value $|\langle\psi_3|\phi\rangle|^2 + |\langle\psi_4|\phi\rangle|^2$ and on the bottom bands the value $|\langle\psi_1|\phi\rangle|^2 + |\langle\psi_2|\phi\rangle|^2$. In the location of the SWPs, the spin S_z of both the valence states ψ_1 and ψ_2 , is all conduction. Even though the 3D BHZ model has an energy gap, at some points in momentum space the spin of the valence states lies on the conduction band. The BHZ models an energy insulator which does not insulate the spin.

In Figure 1 b), it is observed that the SHC exhibits alignment with the ASCN when the spin direction rotates along the k_y axis. In this graph, it is noted that both ASCN and SHC undergo a change in sign from S_z (angle=0) to S_{-z} (angle= π).

In Fig. 2 we have plotted the energy bands on the k_z -axis for $(k_x, k_y) = (0, \pi)$ for specific choice of constants. The SWPs are located on this axis. We have colored the energy bands with the square of the norm of the projection of $S_z|\phi\rangle$ on the valence and the conduction bands where ϕ is the eigenvector of the projected spin operator PS_zP with smallest positive eigenvalue. Note that at the SWPs, the spin of the valence energy states is all conduction. Namely, even though the BHZ models an insulator in terms of its energy spectrum, it is not an insulator on the spin spectrum.

In order to demonstrate the applicability of the current methodology to real-world materials, we have calculated the ASCN and SHC for different topological insulator materials. Here we contrast the results for the case of Bi_2Te_3 , MnBi_2Te_4 , $\text{MnBi}_6\text{Te}_{10}$ and $\alpha\text{-BiBr}$. The calculations were performed using a combination of first-principles methods based on the VASP,³⁰ the Wannier90,³¹ and the Pythtb code,³² with detailed computational setups outlined in the manuscript.¹⁶

We evaluated the electronic and spin spectra of these materials, including the projection of spin projected eigenvalues (PS_zP) onto the electronic bands, as depicted in Fig. 3. For the case of Bi_2Te_3 , we observed a pronounced concentration of valence spin information around a singular point in the conduction band along the ΓT k -path. This localization of spin information suggests the existence of a spin Weyl point along the ΓT path, as depicted in Fig. 3 a). Remarkably, the projected spin spectrum calculation unveils the presence of spin Weyl points both in the TT and $-\text{TT}$ paths, which represent the diagonal direction in the rhombohedral phase or z axis in cartesian coordinates. Consequently, the ASCN is expected to be proportional to the distance between these SWPs, as in the 3D BHZ model. Indeed, we have found that the both ASCN and SHC exhibit a proportional relationship with the SWPs distance. Table I presents the value of ASCN and SHC for Bi_2Te_3 , demonstrating a topological response across all k_z -planes in the hexagonal BZ. Notably, the SHC signal is particularly pronounced along the z -axis, coinciding with the location of SWP in reciprocal space. This result aligns with the layered structure of Bi_2Te_3 , where the z planes correspond to the layers in real space.

TABLE I. Average Spin Chern Number ($\bar{c}_{1,ij}^z$) and Spin Hall Conductance (σ_{ij}^z) values for topological materials Bi_2Te_3 , MnBi_2Te_4 and $\text{MnBi}_6\text{Te}_{10}$ and $\alpha\text{-BiBr}$, where MnBi_2Te_4 and $\text{MnBi}_6\text{Te}_{10}$ are taken in their antiferromagnetic phase. The table includes ASCN and SHC values are given in units of $-e\pi$. The last row classifies the materials as strong topological insulator (STI), axion insulator (AI) or quantum Hall spin insulator (QSHI).

	Bi_2Te_3	MnBi_2Te_4	$\text{MnBi}_6\text{Te}_{10}$	$\alpha\text{-BiBr}$
σ_{yx}^z	3.27	-2.70	-4.48	-3.96
$\bar{c}_{1,xy}^z$	3.16	-2.60	-5.04	-4
σ_{xy}^z	-3.25	2.70	4.48	3.66
Type	STI	AI	AI	QSHI

We have performed an analysis of the electronic and projected spin spectrum of $\alpha\text{-BiBr}$, uncovering a nonzero energy and projected spin gap throughout the entire Brillouin zone. This characteristic serves to classify the $\alpha\text{-BiBr}$ as both an energy and spin insulator, as it shown in Fig. 3 b), in agreement with Lin *et al.*¹⁴ Furthermore, no significant exchange of spin information between the conduction and valence bands is evident. However, we have observed a constant $\bar{c}_{1,xy}^z$ value of -4 along all the k_z planes and zero of the k_x and k_y planes in the Brillouin zone for $\alpha\text{-BiBr}$, which is consistent with the $\sigma_{yx}^z \sim -4$ as presented in Table I. The alignment between SHC and ASCN reflects the full topological response of $\alpha\text{-BiBr}$ perpendicular to the z -axis. This result is hidden for the $\mathbb{Z}_2=0$ index for this material, highlighting the efficacy of ASCN as a tool for extracting valuable insights into the

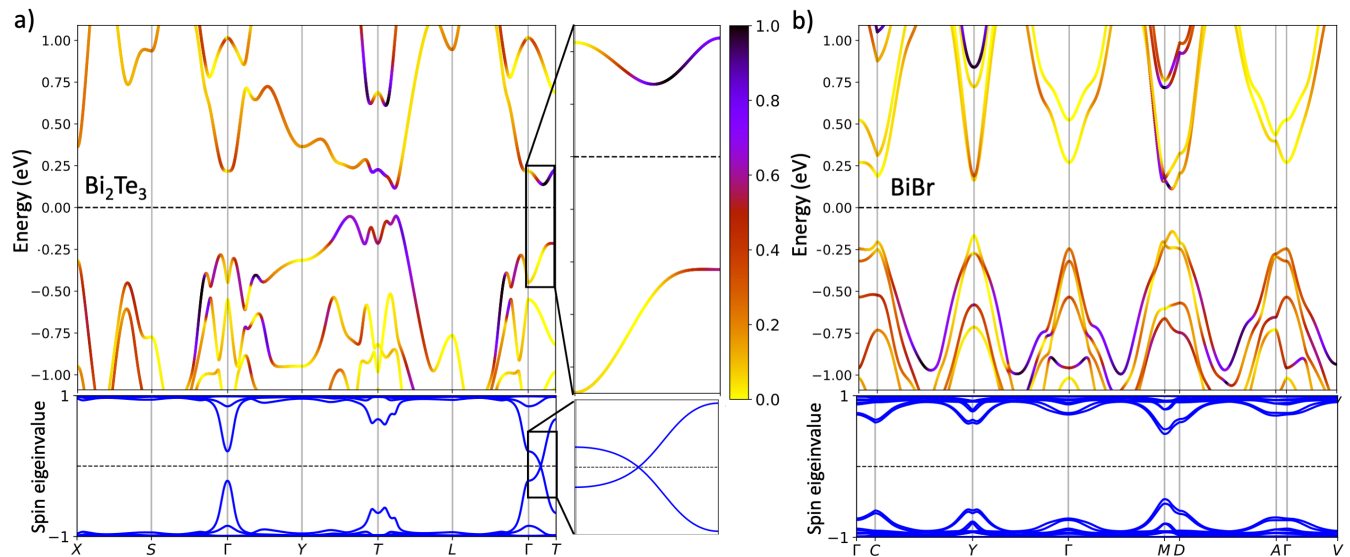


FIG. 3. Energy bands and projected spin S_z eigenvalues for the strong topological insulator Bi_2Te_3 and the weak topological insulator $\alpha\text{-BiBr}$. The color on the energy bands represent the square of the norm of the projection of the smallest positive projected spin eigenvector into each pair of degenerate bands, both valence and conduction. If ϕ is the eigenvector of the smallest positive eigenvalue of PS_zP , the color on each pair of consecutive degenerate bands ψ_{2n-1}, ψ_{2n} is given by the value $|\langle \psi_{2n-1} | S_z \phi \rangle|^2 + |\langle \psi_{2n} | S_z \phi \rangle|^2$. a) Bi_2Te_3 is a strong topological insulator, and as such, it has SWPs on the T- Γ -T path. The chiralities of these SWPs is ± 1 and the ASCN is $c_{1,xy}^{S_z} = 3.16$, which means that the SWPs are located almost in the middle of the T- Γ path. Note that the value of the intrinsic SHC is $\sigma_{yx}^z = 3.27$ which is very close to the ASCN. The eigenvector of the projected spin operator with smallest positive eigenvalue is entirely conduction on the SWPs. This can be seen in the Γ -T path. b) $\alpha\text{-BiBr}$ is a spin Chern insulator since the value of the ASCN $c_{1,xy}^{S_z} = -4$ is a non-zero even integer. The spin insulation can be read from the fact that the ASCN is an even integer, and the topological feature is given by the constant value of -4 for the SCN on the $k_x k_y$ planes. Since this SCN is a multiple of 4, the Chern number of the positive and negative projected spin eigenvectors is equal to 2 and -2 respectively. Hence the number of pairs of negative eigenvalues of the inversion operator is even and therefore the strong topological insulator marker \mathbb{Z}_2 of Fu-Kane-Mele is equal to zero. This shows how the ASCN adds information for the classification of topological features on materials.

spin response of topological insulators.

It is found that $\alpha\text{-BiBr}$ displays a vanishing ASCN for the S_x and S_y spin components, suggesting a lack of topological response in SHC for these spin directions. Our calculations confirm $\alpha\text{-BiBr}$ as a 3D quantum spin Hall insulator (S_z). The observed anisotropy between σ_{xy}^z and σ_{yx}^z responses is further supported by symmetry analysis of the SHC tensor, indicating distinct components within this space group (#12). This convergence of ASCN and SHC values highlights the unique topological nature of $\alpha\text{-BiBr}$.

Regarding the axion insulators (AI) MnBi_2Te_4 and $\text{MnBi}_6\text{Te}_{10}$, we also see that the values of the ASCN and SHC are very similar. In these two materials time reversal coupled with a translation is a preserved symmetry, and therefore the Chern numbers of the positive and negative projected spin eigenvectors are inverse to one another. Therefore we can conclude that the spin Chern number on all k_z planes for MnBi_2Te_4 are less than -2 and for $\text{MnBi}_6\text{Te}_{10}$ are less than -4 .

With the SHC alone we may not distinguish the materials in Table I, but with the incorporation of the ASCN we differentiate $\alpha\text{-BiBr}$ from the others. The incorpo-

ration of the ASCN into the set of material classifiers will help distinguish QSHIs from strong topological and axion insulators, and moreover, it will permit to distinguish the topological features underlying the projected spin operator.

It is also important to remark that the ASCN calculations are significantly less intensive compared to SHC calculations. The former needs 3D dense k -grids while the latter only needs a dense k -grid in one dimension. The ASCN can also be calculated in collinear ferromagnetic or antiferromagnetic when the spin z component can be consider a good quantum number in the weak SOC limit. These results indicate the practical advantage of employing ASCN as a computational tool and topological indicator, in scenarios where the efficient calculation of SHC is limited.

ACKNOWLEDGMENTS

The first author gratefully acknowledges the computing time granted on the supercomputer Mogon at Johannes Gutenberg University Mainz (hpc.uni-mainz.de).

The second author acknowledges the support of CONACYT through project CB-2017-2018-A1-S-30345-F-3125 and of the Max Planck Institute for Mathematics in Bonn, Germany. Both authors thank the continuous support of the Alexander Von Humboldt Foundation, Germany.

* rhernandezj@uninorte.edu.co

† bjongbloed@uninorte.edu.co

- [1] D. J. Thouless, M. Kohmoto, M. P. Nightingale, and M. den Nijs, Phys. Rev. Lett. **49**, 405 (1982), URL <https://link.aps.org/doi/10.1103/PhysRevLett.49.405>.
- [2] F. D. M. Haldane, Phys. Rev. Lett. **61**, 2015 (1988), URL <https://link.aps.org/doi/10.1103/PhysRevLett.61.2015>.
- [3] J. Sinova, S. O. Valenzuela, J. Wunderlich, C. Back, and T. Jungwirth, Reviews of Modern Physics **87**, 1213 (2015).
- [4] C. L. Kane and E. J. Mele, Physical Review Letters **95**, 226801 (2005).
- [5] M. Z. Hasan and C. L. Kane, Reviews of Modern Physics **82**, 3045 (2010).
- [6] X.-L. Qi and S.-C. Zhang, Review of Modern Physics **83**, 1057 (2011).
- [7] X.-L. Qi, T. L. Hughes, and S.-C. Zhang, Physical Review B **78**, 195424 (2008).
- [8] R. Chen and B. Zhou, Physics Letters A **381**, 944 (2017), ISSN 0375-9601, URL <https://www.sciencedirect.com/science/article/pii/S0375960117300737>.
- [9] F. Matusalem, M. Marques, L. K. Teles, L. Matthes, J. Furthmüller, and F. Bechstedt, Phys. Rev. B **100**, 245430 (2019), URL <https://link.aps.org/doi/10.1103/PhysRevB.100.245430>.
- [10] S. M. Farzaneh and S. Rakheja, Phys. Rev. Mater. **4**, 114202 (2020), URL <https://link.aps.org/doi/10.1103/PhysRevMaterials.4.114202>.
- [11] M. G. Vergniory, B. J. Wieder, L. Elcoro, S. S. P. Parkin, C. Felser, B. A. Bernevig, and N. Regnault, Science **376**, eabg9094 (2022), <https://www.science.org/doi/pdf/10.1126/science.abg9094>, URL <https://www.science.org/doi/abs/10.1126/science.abg9094>.
- [12] B. Bradlyn, L. Elcoro, J. Cano, M. G. Vergniory, Z. Wang, C. Felser, M. I. Aroyo, and B. A. Bernevig, Nature **547**, 298 (2017), ISSN 1476-4687, URL <https://doi.org/10.1038/nature23268>.
- [13] E. Prodan, Phys. Rev. B **80**, 125327 (2009), URL <https://link.aps.org/doi/10.1103/PhysRevB.80.125327>.
- [14] K.-S. Lin, G. Palumbo, Z. Guo, Y. Hwang, J. Blackburn, D. P. Shoemaker, F. Mahmood, Z. Wang, G. A. Fiete, B. J. Wieder, et al., Nature Communications **15**, 550 (2024), ISSN 2041-1723, URL <https://doi.org/10.1038/s41467-024-44762-w>.
- [15] G. F. Lange, A. Bouhon, and R.-J. Slager, Phys. Rev. Res. **5**, 033013 (2023), URL <https://link.aps.org/doi/10.1103/PhysRevResearch.5.033013>.
- [16] R. González-Hernández and B. Uribe, Phys. Rev. B **109**, 045126 (2024), URL <https://link.aps.org/doi/10.1103/PhysRevB.109.045126>.
- [17] M. Asorey, Nature Physics **12**, 616 (2016), ISSN 1745-2481, URL <https://doi.org/10.1038/nphys3800>.
- [18] X.-L. Qi, T. L. Hughes, and S.-C. Zhang, Phys. Rev. B **78**, 195424 (2008), URL <https://link.aps.org/doi/10.1103/PhysRevB.78.195424>.
- [19] A. M. Essin, J. E. Moore, and D. Vanderbilt, Phys. Rev. Lett. **102**, 146805 (2009), URL <https://link.aps.org/doi/10.1103/PhysRevLett.102.146805>.
- [20] N. Varnava and D. Vanderbilt, Phys. Rev. B **98**, 245117 (2018), URL <https://link.aps.org/doi/10.1103/PhysRevB.98.245117>.
- [21] R. Moessner and J. E. Moore, *Topological Phases of Matter* (Cambridge University Press, 2021).
- [22] L. Fu and C. L. Kane, Phys. Rev. B **74**, 195312 (2006), URL <https://link.aps.org/doi/10.1103/PhysRevB.74.195312>.
- [23] L. Fu, C. L. Kane, and E. J. Mele, Phys. Rev. Lett. **98**, 106803 (2007), URL <https://link.aps.org/doi/10.1103/PhysRevLett.98.106803>.
- [24] R. González-Hernández and B. Uribe, Supplemental material (2024).
- [25] Y. Bai, L. Cai, N. Mao, R. Li, Y. Dai, B. Huang, and C. Niu, Phys. Rev. B **105**, 195142 (2022), URL <https://link.aps.org/doi/10.1103/PhysRevB.105.195142>.
- [26] M. König, S. Wiedmann, C. Brüne, A. Roth, H. Buhmann, L. W. Molenkamp, X.-L. Qi, and S.-C. Zhang, Science **318**, 766 (2007), <https://www.science.org/doi/pdf/10.1126/science.1148047>, URL <https://www.science.org/doi/abs/10.1126/science.1148047>.
- [27] A. A. Burkov, Phys. Rev. Lett. **113**, 187202 (2014), URL <https://link.aps.org/doi/10.1103/PhysRevLett.113.187202>.
- [28] Z. Fang, N. Nagaosa, K. S. Takahashi, A. Asamitsu, R. Mathieu, T. Ogasawara, H. Yamada, M. Kawasaki, Y. Tokura, and K. Terakura, Science **302**, 92 (2003), ISSN 0036-8075, <https://science.sciencemag.org/content/302/5642/92.full.pdf>, URL <https://science.sciencemag.org/content/302/5642/92>.
- [29] B. A. Bernevig, T. L. Hughes, and S.-C. Zhang, Science **314**, 1757 (2006), <https://www.science.org/doi/pdf/10.1126/science.1133734>, URL <https://www.science.org/doi/abs/10.1126/science.1133734>.
- [30] G. Kresse and J. Furthmüller, Phys. Rev. B **54**, 11169 (1996), URL <https://link.aps.org/doi/10.1103/PhysRevB.54.11169>.
- [31] A. A. Mostofi, J. R. Yates, G. Pizzi, Y.-S. Lee, I. Souza, D. Vanderbilt, and N. Marzari, Computer Physics Communications **185**, 2309 (2014), ISSN 0010-4655, URL <http://www.sciencedirect.com/science/article/pii/S001046551400157X>.
- [32] *Python tight binding open-source package*, <http://physics.rutgers.edu/pythtb>.